A Frequency-domain Approach to Noninvasive Intracranial Pressure Estimation

Rohan Jaishankar[1], *Student Member, IEEE*, Andrea Fanelli[2], *Member, IEEE*, Aristotelis Filippidis[3], Thai Vu[3], James Holsapple[3], and Thomas Heldt[4], *Senior Member, IEEE*

***Abstract*— Intracranial pressure (ICP) is a cranial vital sign, crucial in the monitoring and treatment of several neurological injuries. The clinically accepted measurement modalities of ICP are highly invasive, carrying risks of infection and limiting the benefits of ICP measurement to a small subset of critically ill patients. This work aims to take a step towards developing an accurate noninvasive means of estimating ICP, by utilizing a model-based frequency-domain approach. The mean ICP and pulse pressures of ICP are estimated from arterial blood pressure (ABP) and cerebral blood flow velocity (CBFV) waveforms, and the estimates are validated on an adult population, comprising of around two hours of data from five patients. The algorithm was shown to have an accuracy (mean error) of -1.5 mmHg and a precision (standard deviation of the error) of 4.3 mmHg in estimating the mean ICP. These results are comparable to the previously reported errors among the currently accepted invasive measurement methods, and well within the clinically relevant range.**

I. INTRODUCTION

A sizeable fraction of the annual hospitalizations in the United States are due to a variety of neurological and cerebrospinal injuries and disorders [1]. Each year around 2.8 million people suffer a traumatic brain injury (TBI) [2], over 100,000 people suffer a hemorrhagic stroke [3], and nearly 80,000 new cases of brain tumor are reported [4]. In a subset of these patients, measurement of the intracranial pressure (ICP) is clinically indicated to detect, monitor, and treat acutely life-threatening conditions. Such conditions may arise because of poor brain perfusion with elevated ICP or brain herniation [5], [6]. Current measurement modalities, however, are invasive, involving the insertion of a catheter or pressure transducer into the cerebrospinal fluid space or the brain tissue, respectively, thereby exposing patients to the risk of tissue damage and infection [7]. There remains a significant need for noninvasive determination and continuous tracking of ICP.

This study was supported in part by Philips Healthcare.

[1]Rohan Jaishankar is with the Institute of Medical Engineering & Sciences and the Department of Electrical Engineering & Computer Science, Massachusetts Institute of Technology, Cambridge, MA 02139 USA.

[1]Andrea Fanelli is with the Institute for Medical Engineering & Science and the Research Laboratory of Electronics, Massachusetts Institute of Technology, Cambridge, MA 02139 USA.

[3]Aristotelis Filippidis, Thai Vu, and James Holsapple are with the Department of Neurosurgery, Boston Medical Center, Boston, MA 02118 USA.

[4]Thomas Heldt is with the Institute for Medical Engineering & Science, Research Laboratory of Electronics, and Department of Electrical Engineering & Computer Science, Massachusetts Institute of Technology, Cambridge, MA 02139 USA. thomas@mit.edu

Kashif *et al.* [8] proposed a model-based approach to estimate ICP continuously and noninvasively from arterial blood pressure (ABP) and cerebral blood flow velocity (CBFV) waveform signals, and the authors chose to solve the estimation problem in the time domain. Noraky *et al.* [9] extended this prior work and formulated a frequency-domain approach to ICP estimation. Both approaches had limitations that may have impacted their accuracy and robustness. The time-domain approach had the inherent limitation of needing to estimate the phase lag between the cerebral ABP and CBFV signals. This limitation motivated the explorations by Noraky *et al.* [9]. Here, we build on these past model-based ICP estimation approaches and seek to address their limitations.

II. MATERIALS AND METHODS

A. Model of cerebrovascular physiology

Building on the prior work Noraky *et al.* [9], we utilize a second-order lumped parameter circuit model (Fig. 1) to represent a major cerebral vascular territory, such as the middle cerebral artery (MCA). Here, $p_a(t)$ represents the cerebral ABP, $q(t)$ represents the cerebral blood flow (CBF), and p_{ic} represents the ICP. R captures the resistance to blood flow through the vascular territory, C models the lumped compliance of the vessel wall and surrounding brain tissue, and L represents the inertia of blood [10]. The cerebral blood flow is driven in the model by the difference between ABP and ICP, known as the cerebral perfusion pressure (CPP), which we will denote here as $x(t)$.

$$CPP = p_a(t) - p_{ic} = x(t) \tag{1}$$

The circuit model in Fig. 1 is described mathematically

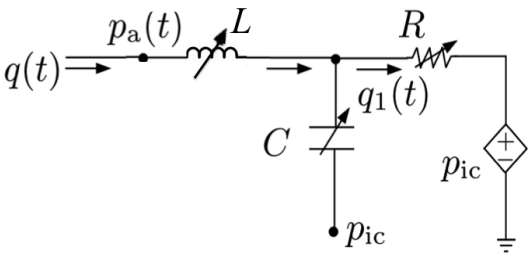

Fig. 1: Second-order circuit model used to noninvasively estimate ICP, bulding upon the model proposed by Noraky *et al.* [9].

by

$$q(t)+\frac{L}{R}\frac{dq(t)}{dt}+LC\frac{d^2q(t)}{dt^2}=\frac{x(t)}{R}+C\frac{dx(t)}{dt} \quad (2)$$

It can be shown that this circuit equation is invariant to multiplicative scaling of $q(t)$, by rescaling of R, L and C [**?**]. By scaling the circuit equation by a constant factor to account for the effective arterial cross-sectional area, the CBF can be transformed to the CBFV, which is physically measurable by means of a transcranial Doppler (TCD) ultrasound device. Henceforth, $q(t)$ will refer to this CBFV waveform, while R, L and C will represent the transformed versions of the respective parameters.

The frequency-domain representation of Equation 2 is given by

$$|Q(j\omega)|^2[(1-\omega^2LC)^2+(\frac{\omega L}{R})^2]=|X(j\omega)|^2[\frac{1}{R^2}+(\omega C)^2] \quad (3)$$

The use of power spectra to solve the constraint implied by these differential equations overcomes the primary limitation of the time-domain approach as the phase lag between the input waveforms does not need to be estimated [9], [10].

For estimating ICP, ABP and CBFV waveform data are first divided into non-overlapping windows of 60 beats duration. The values of the three circuit parameters (R, L and C) and the ICP are assumed to be constant over each estimation window. Hence, the algorithm returns a single estimate of mean ICP every 60 beats. Ideally, the scaled parameters R, L and C can be estimated from Equation 3 using a least-squares optimization at appropriately computed harmonic frequencies of the heart rate. However, the CPP power spectrum, $|X(j\omega)|^2$, is unknown as it requires knowledge of the ICP waveform which has to be ultimately estimated.

B. ICP and CPP reconstruction

Careful inspection of the dynamics between the mean-subtracted ABP and ICP waveforms on a beat-by-beat basis resulted in the observation that they tend to conform to a characteristic shape (Fig. 2). To determine the ICP waveform

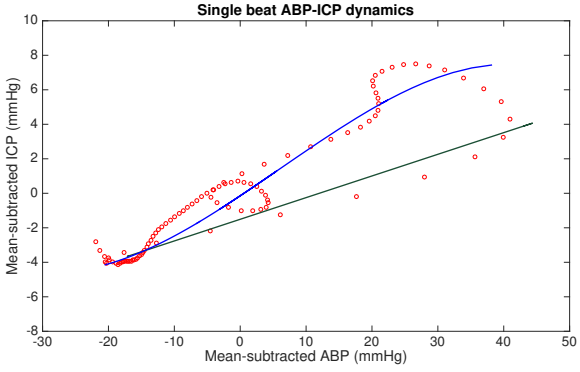

Fig. 2: Representative example of a single-beat dynamics between mean-subtracted ABP and the corresponding mean-subtracted ICP. There are two clear phases: a systolic upstroke (blue line) and a diastolic decay (black cubic polynomial).

variation from the available ABP waveform variation, we modeled the systolic (upstroke) and diastolic (downstroke) phases of the ABP-ICP relationship according to a linear relationship and a cubic spline, respectively.

$$p_{ic_{up}}(t) = p_{up}(t)*\alpha_{up}+\beta_{up} \quad (4)$$

$$p_{ic_{down}}(t) = \beta_d+\sum_{i=1}^{3}p^i_{down}(t)*\alpha_{id} \quad (5)$$

$$p_{ic_{recon}}(t) = [p_{ic_{up}}(t) \quad p_{ic_{down}}(t)] \quad (6)$$

$$x_{recon}(t) = p(t)-p_{ic_{recon}}(t) \quad (7)$$

A small portion of a separate pediatric clinical dataset available to us was used as a training dataset to compute fitting parameters α_{up} and β_{up} for the upstroke (blue line in Fig. 2), and α_{1d}, α_{2d}, α_{3d} and β_d for the downstroke (black line in Fig. 2). The mean-subtracted ICP waveform, and hence the intra-beat variations in CPP, are then reconstructed ($p_{ic_{recon}}(t)$) over each estimation window for all the data records, using the fitting parameters and corresponding ABP waveform phases ($p_{up}(t)$ for upstroke and $p_{down}(t)$ for the downstroke).

C. ICP estimation

The power spectra of the mean-subtracted CBFV, $Q(j\omega)|^2$, and reconstructed CPP, $|X(j\omega)|^2$, waveforms are computed over each estimation window, using a Hamming-window based averaged periodogram method over two sub-windows. Eight spectral peaks are selected in both spectra using a scanning technique around the harmonics of the heart rate. These eight frequency locations are then used to formulate Equation 3 in a least-squares sense. The least-squares optimization is solved to yield parameter estimates $\widehat{R}$, $\widehat{L}$ and $\widehat{C}$ over each estimation window. Finally, the noninvasive estimate of mean ICP is computed over each estimation window as

$$\widehat{nICP}=\overline{p_w}-\widehat{R}\,\overline{q_w} \quad (8)$$

where $\overline{p_w}$ and $\overline{q_w}$ denote the window-averaged ABP and CBFV, respectively.

D. Signal preprocessing and hydrostatic pressure correction

The ABP and CBFV waveforms used for validating our algorithm were collected from adults in the neuro-ICU and hence were prone to noise and several artifacts. As a result, a previously developed automated preprocessing pipeline [11], [12] was implemented to scan through the ABP and CBFV data and select segments where both waveforms were of good signal quality. These segments were then manually inspected to remove any potential visually distinguishable artifacts. Finally, an 80-tap finite impulse response (FIR) bandpass filter, with pass band cutoffs at 0.5 Hz and 12 Hz was used to filter both waveforms.

At the bedside, ABP is routinely recorded by cannulation of the radial artery in patients with the pressure transducer levelled to the position of the heart. However, since the patients are maintained in a head-up position, we had to correct the ABP to the level of the MCA (represented by

our model) by subtracting the effective vertical column of blood between the two measurement locations.

$$ABP_{\text{MCA}} = ABP_{\text{radial}} - \rho_{\text{blood}} * g * (h_{\text{MCA}} - h_{\text{radial}}) \quad (9)$$

The density of blood ρ_{blood} was taken to be 1060 kg/m^3. The values of h_{MCA} and h_{radial} were recorded as the vertical heights of the ICP and ABP transducers, respectively, as measured from the floor.

E. Clinical Dataset

We designed and deployed a custom data acquisition system in the neuro-ICU at Boston Medical Center (BMC) to collect high fidelity waveform and ancillary data from adult patients admitted with a variety of neurological insults [13]. The data collection was approved by the Institutional Review Boards at BMC and MIT, and informed consent was obtained from the patient or their legally authorized representative. The recorded data had to satisfy several criteria to serve as inputs to our estimation algorithm for validation. Briefly, the basic requirements were the presence of a radial arterial line for invasive ABP measurement, the invasive measurement of ICP by either an external ventricular drain or parenchymal probe, and the recording of important ancillary data from the bedside such as the vertical heights of pressure transducers. CBFV data were recorded using either the DWL Doppler BoxX or the Philips CX-50 ultrasound devices, while the ABP and ICP waveforms and vital signs were streamed to our system from the GE Solar 8000i patient monitors through the GE TramRac 4A. After passing the data through the signal preprocessing pipeline and manually rejecting artifacts, a total of one hour and 48 minutes of good quality data were selected from five patients (4 male, 1 female), for analysis of our estimation algorithm in this study. The patients ranged in age from 20 to 74 years and were hospitalized for severe TBI (3 patients), brain tumor (1 patient), and acute hydrocephalus (1 patient).

III. RESULTS

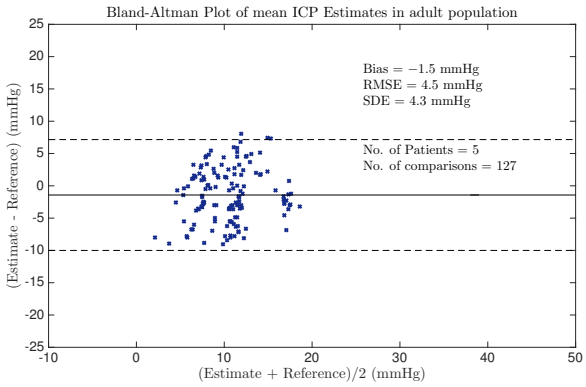

Fig. 3: Bland-Altman plot comparing estimated and measured mean ICP on a window-by-window basis in an adult population.

We estimated mean ICP over 60-beat windows and pulse pressure over each beat, and compared these estimated to those of the clinically measured invasive ICP. The resultant estimates for mean ICP had a bias of −1.5 mmHg, a root mean-squared error (RMSE) of 4.5 mmHg and a SDE of 4.3 mmHg. These results are summarized in the Bland-Altman plot [14] shown in Fig. 3.

The spread of the algorithm's performance was also inspected, to compute the number of estimates falling below a RMSE threshold, on a window-by-window, study-by-study and patient-by-patient basis. The cumulative RMSE distribution functions generated by varying this RMSE threshold are shown in Fig. 4. Around 80% of the estimation results fell below a RMSE threshold of 6 mmHg on a window-by-window basis.

IV. DISCUSSION

We analyzed the performance of our estimation algorithm on five adult patients and the resultant accuracy and precision of −1.5 mmHg and 4.3 mmHg, respectively, are highly encouraging. These errors are well within the clinically acceptable range for ICP measurement and also compare favorably to some of the previously reported errors in comparing invasive ICP measurement modalities. While the EVDs and parenchymal probes are commonly used, past studies have shown errors in agreement between the probes. Lescot *et al.* reported limits of agreement of (−8.1 mmHg, 6.9 mmHg) and (−6.7 mmHg, 7.1 mmHg) when comparing 15 instances of two different parenchymal probes to a reference EVD measurement [15]. These error metrics are in the same range as our algorithm's limits of agreement of (−9.9 mmHg, 6.9 mmHg). Brean *et al.* reported a bias of 0.7 mmHg and a standard deviation of the error of 6.8 mmHg, when comparing simultaneous EVD and intraparenchymal ICP measurements in one subarachnoid hemorrhage patient [17]. Other systematic reviews of the different ICP modalities have also been documented, reporting errors and drawbacks of each of the methods [7], [18]. It is highly encouraging that our estimation results are comparable to the currently accepted clinical invasive standards.

Our algorithm also has the advantage of being calibration-free and robust. The fitting parameters for the ABP-ICP

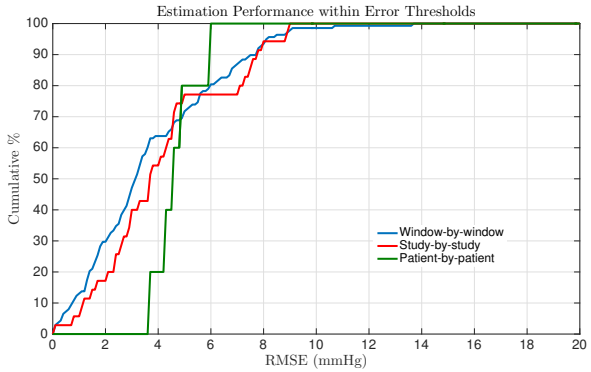

Fig. 4: Percentage of mean nICP estimates below a RMSE threshold. The analysis is carried out on a per-window, per-study, and per-patient basis.

dynamics were obtained on a small portion of an independent pediatric clinical dataset. We were completely blinded to all the ICP waveforms in the dataset, proving the robustness of the algorithm. Our algorithm also performed very well on patients from a diverse range of ages and neurological pathologies.

However, our algorithm and the analysis presented in this study have some limitations and scope for further work. Primarily, the amount of clinical data available to us in this study was highly limited. While the results on different pathologies are encouraging, it is imperative to validate our results on a larger patient population, demonstrating further diversity in demographics and pathologies. We continue to work towards this end as the data collection at BMC is ongoing. Another practical limitation of our work is the use of radial ABP as a surrogate for the MCA ABP. These two waveforms potentially have morphological differences, apart form the hydrostatic compensation we accounted for. Finally, the homogeneity of the clinical dataset with respect to the ICP values poses a challenge. Patients in the neuro-ICU are constantly monitored and their ICP is controlled to remain within normal ranges. As a result, we were so far unable to test our algorithm's accuracy on ICP values above 25 mmHg or on patients with sustained intracranial hypertension.

V. CONCLUSIONS

ICP serves as a crucial indicator in assisting physicians in clinical decision-making and in guiding treatment of patients with neurological injuries. However, the current ICP measurement modalities are highly invasive and hence there is a pressing need to develop a noninvasive ICP measurement technique, to expand the patient pool who could benefit from the monitoring of this cranial vital sign. In this study, we took a step towards solving this problem by developing and implementing a frequency-domain, model-based, non-invasive ICP estimation algorithm. We analyzed the results on a clinical dataset of five adult patient and obtained an accuracy of -1.5 mmHg and a precision of 4.3 mmHg. The algorithm performance is encouraging, and further validation in an expanded dataset is warranted.

REFERENCES

[1] C.L. Gooch *et al. The Burden of Neurological Disease in the United States: A Summary Report and Call to Action.* Annals of Neurology, 81(4): 479-484, 2017.

[2] C.A. Taylor *et al. Traumatic Brain Injury-Related Emergency Department Visits, Hospitalizations, and Deaths - United States, 2007 and 2013.* MMWR Surveillance Summary, 66(9):1-16, 2017.

[3] E.J. Benjamin *et al. Heart Disease and Stroke Statistics 2018 update: A Report from the American Heart Association.* Circulation, 137: 67-492, 2018.

[4] American Brain Tumor Association. *http://www.abta.org/about-us/news/brain-tumor-statistics/.* Accessed May 8, 2018.

[5] L.A. Steiner and P.J.D. Andrews. *Monitoring the injured brain: ICP and CBF*. British Journal of Anaesthesia, 97(1): 26-38, 2006.

[6] J.D. Miller *et al. Significance of intracranial hypertension in severe head injury.* Journal of Neurosurgery, 47: 503-516, 1977.

[7] X. Zhang *et al. Invasive and noninvasive means of measuring intracranial pressure: a review.* Physiological Measurement, 38(8):143-182, 2017.

[8] F.M. Kashif *et al.Model-based noninvasive estimation of intracranial pressure from cerebral blood flow velocity and arterial pressure.* Science Translational Medicine, 4(129): 129-144, 2012.

[9] J. Noraky *et al. Noninvasive Intracranial Pressure Determination in Patients with Subarachnoid Hemorrhage.* Acta neurochirurgica. Supplement, 122:65-68, 2016.

[10] R. Jaishankar. *A Spectral Approach for Noninvasive Estimation of Intracranial Pressure*. SM thesis, Department of Electrical Engineering and Computer Science, Massachusetts Institute of Technology, 2017.

[11] A. Fanelli and T. Heldt. *Signal quality quantification and waveform reconstruction of arterial blood pressure recordings.* Conference Proceedings of IEEE Engineering and Medicine in Biology Society 2014:2233-2236, 2014.

[12] F. Wadehn *et al. Segmentation of TCD Cerebral Blood Flow Velocity Recordings.* 2018; Available from: http://arxiv.org/abs/1806.09994.

[13] A. Fanelli *et al. A Waveform Archiving System for the GE Solar 8000i Bedside Monitor.* Acta neurochirurgica. Supplement, 126:173-177, 2018.

[14] J.M. Bland and D.G. Altman.*Statistical methods for assessing agreement between two methods of clinical measurement.* Lancet, 1(8476):307-310, 1986.

[15] T. Lescot *et al. In vivo accuracy of two intraparenchymal intracranial pressure monitors.* Intensive Care Medicine, 37:875-879, 2011.

[16] C. Weigand and P. Richards. *Measurement of intracranial pressure in children: a critical review of current methods.* Developmental Medicine and Child Neurology, 49(12):935-941, 2007.

[17] A. Brean *et al. Comparison of intracranial pressure measured simultaneously within the brain parenchyma and cerebral ventricles.* Journal of Clincial Monitoring and Computing, 20:411-414, 2006.

[18] L. Zacchetti *et al. Accuracy of intracranial pressure monitoring: systematic review and meta-analysis.* Critical Care, 19:420, 2015.